WCTE 2016
World Conference on Timber Engineering
August 22-25, 2016 | Vienna, Austria

Numerical modelling of steel-to-timber joints and connectors for CLT structures

Matteo Izzi[1], Giovanni Rinaldin[2], Massimo Fragiacomo[3], Andrea Polastri[4]

ABSTRACT: The mechanical behaviour of steel-to-timber joints with annular-ringed shank nails is investigated using numerical modelling and a component approach. These joints are used in Cross-Laminated Timber (CLT) buildings to anchor metal connectors such as hold-downs and angle brackets to the timber panels. At first, a general hysteresis model is introduced, where a single fastener joint is schematized as an elasto-plastic beam embedded in a non-linear medium with a compression-only behaviour. A second hysteresis model is then presented, where the mechanical behaviour of the joint is simulated by a non-linear spring with three degrees of freedom. Both models are calibrated on the design rules prescribed by the reference standards. Moreover, average strength capacities are determined from the corresponding characteristic values assuming a standard normal distribution and suitable coefficients of variation. As first applicative examples of the proposed models, shear tests are simulated on single steel-to-timber joints with annular-ringed shank nails and on a connection made of an angle bracket and sixty nails. The scatter of mechanical properties in steel-to-timber joints is also taken into account in the simulations and a stochastic approach is proposed, demonstrating acceptable accuracy.

KEYWORDS: steel-to-timber joint, dowel-type fastener, metal connector, non-linear modelling, component approach

1 INTRODUCTION

In this paper, two new numerical models for the prediction of the mechanical behaviour of steel-to-timber joints and metal connector for CLT structures are proposed.

At first, a general hysteresis model for the prediction of the mechanical behaviour of single steel-to-timber fastener is presented. The model (M1-model in the following) schematizes a joint with a dowel-type fastener as an elasto-plastic beam embedded in a non-linear medium with a compression-only behaviour.

The non-linear behaviour of the single fastener joint is simulated in the M1-model by means of non-linear spring elements that govern (*a*) the bending behaviour of the fastener, (*b*) the embedment response in compression of timber and (*c*) the withdrawal resistance of the fastener. Using basic mechanical properties of the fastener and the physical properties of timber, the model is able to predict the non-linear behaviour of the joint under monotonic or cyclic loads and to simulate the pinching effect caused by the gaps that occur in cyclic tests between the supporting medium and the fastener.

A second hysteresis model is proposed afterwards. This second model (in the following referred to as the M2-model) schematizes a steel-to-timber joint as a two-node spring element with three degrees of freedom (3 d.o.f.). Here, the spring is used to simulate the shear behaviour in parallel and perpendicular to the grain direction (2 d.o.f.) and the withdrawal resistance under axial loads (1 d.o.f.).

The M2-model can be calibrated either on the results obtained with other hysteresis models (such as the M1-model) or on calculated strength and stiffness properties determined either from analytical formulations or from experimental results. Furthermore, it can be employed to analyse steel-to-timber connections where many fasteners are used, e.g. a hold-down or an angle bracket.

As first applicative examples of the proposed models, shear tests are simulated on single steel-to-timber joints with Simpson Strong-Tie annular-ringed shank nails and on a connection assembled with a Rothoblaas TTF200 angle bracket and sixty nails. Results of these studies are compared to similar setups experimentally tested. The scatter of mechanical properties is also taken into account and a stochastic approach is proposed. The non-linear spring elements considered in the study are simulated by means of an user element subroutine (UEL) taken from [16]. The piecewise-linear laws used in the paper were derived from the hysteresis models published in the same article.

Strength and stiffness degradation in steel-to-timber joints were not taken into account in current simulations but will be considered and properly simulated in future developments of this study.

[1] Matteo Izzi, University of Trieste, CNR IVALSA, Italy.
E-mail: izzimatteo@gmail.com
[2] Giovanni Rinaldin, University of Sassari, Italy.
E-mail: grinaldin@uniss.it
[3] Massimo Fragiacomo, University of L'Aquila, Italy.
E-mail: massimo.fragiacomo@univaq.it
[4] Andrea Polastri, CNR IVALSA, Italy.
E-mail: polastri@ivalsa.cnr.it

2 M1-MODEL DESCRIPTION

The joint is simulated as an elasto-plastic beam in a non-linear medium characterized by a compression-only behaviour. Using basic mechanical properties of the fastener (ultimate tensile strength) and the physical properties of timber (density), the M1-model is able to predict the mechanical behaviour of a laterally loaded steel-to-timber joint under monotonic or cyclic loads. Moreover, due to the absence of tensile stresses at the interface between timber and fastener, the model is able to simulate the pinching effect caused by the gaps formed between supporting medium and fastener.
A preliminary version of the model can be found in [15]. Results obtained on single steel-to-timber joints could be employed to analyse systems where many of such joints are present. For instance, results obtained on nailed steel-to-timber joints could be implemented in a more general model (using, for instance, the M2-model discussed in Section 3) to predict the behaviour of a metal connector like a hold-down or an angle bracket.

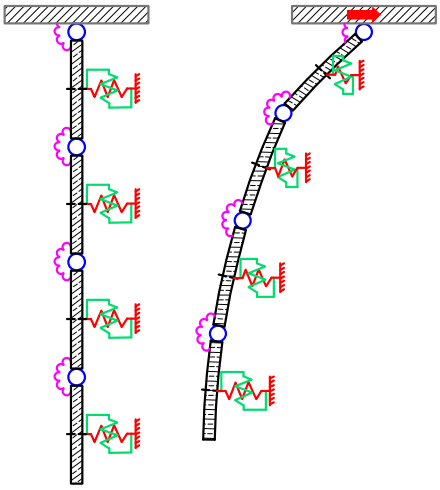

Figure 1: *Schematics of a steel-to-timber joint simulated with the M1-model (left: un-deformed view; right: plastic deformed configuration).*

2.1 FASTENER'S SCHEMATIZATION

Figure 1 represents the schematics of a steel-to-timber joint with a dowel-type fastener. The fastener shank is simulated with non-linear beam elements (of length l) interconnected with hinges (blue circles). Each beam is characterized by an elastic behaviour in bending and a rigid-plastic behaviour in the axial direction. This uncoupled behaviour is achieved by considering the 2nd order effects (i.e. by activating the non-linear geometry), and is used to keep the length of the fastener constant once it assumes its plastic deformed configuration.
The bending behaviour of the fastener is controlled by a set of rotational springs (in magenta), restrained to the ends of two consecutive beam elements. The clamping of the fastener cap to the metal plate is also accounted in the model with an additional spring, located between the upper beam and the metal element.

The rotational springs have an elasto-plastic moment-rotation relationship with elastic stiffness K_θ and yield moment M_y (Figure 2). The stiffness K_θ is determined by assuming that the yield moment M_y is achieved at a maximum rotation of 0.01 deg. The inelastic branch has a hardening behaviour, determined by assuming that the yield moment at the ultimate rotation θ_u (with $\theta_u = 45°$) is 5% higher than M_y.

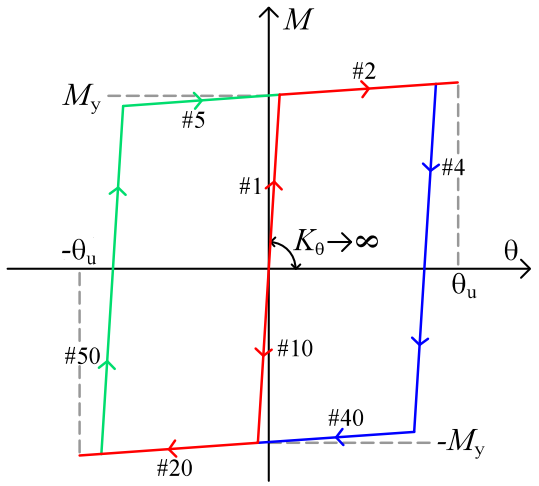

Figure 2: *Bending behaviour of the fastener: piecewise-linear law of the rotational springs (backbone curve in red, unloading path in blue and reloading path in green).*

2.2 EMBEDMENT RESPONSE OF TIMBER

The embedment behaviour of timber in compression is simulated with non-linear springs uniformly distributed along the fastener shank (red springs in Figure 1). Each spring is restrained to a master node, located in the centre of the beam where it is attached and to a fixed point of the surrounding space.
To limit the computational effort required to carry out the simulations, the embedment behaviour in front of and behind each beam is simulated with a unique spring.

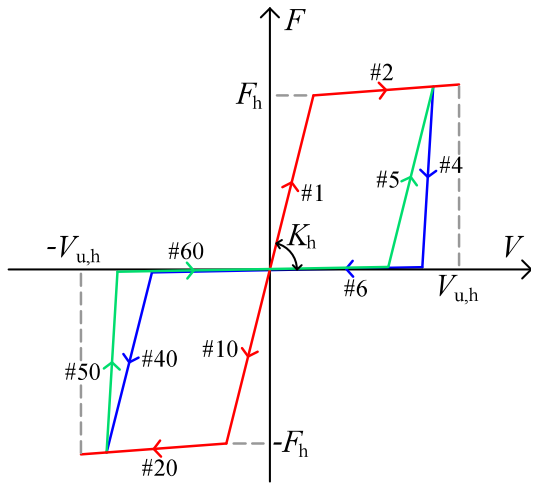

Figure 3: *Embedment behaviour of timber in compression: piecewise-linear law of the non-linear springs (backbone curve in red, unloading path in blue and reloading path in green).*

These springs have an elasto-plastic force-displacement relationship with elastic stiffness K_h and embedding load F_h (Figure 3); the inelastic branch of the backbone curve has a hardening behaviour, determined by assuming that the strength at the ultimate displacement $V_{u,h}$ is 5% higher than F_h (with $V_{u,h}$ set to 10 times the yield displacement).
If the spring is unloaded from a positive displacement, branch #4 is followed until the attainment of zero force; branch #6 simulates the gap between the supporting medium and the fastener. Finally, branch #40 takes to the opposite side of the backbone curve. The slope of #4 and #5 are determined as a function of the stiffness K_h. Without the support of experimental data, the slope of #5 is assumed equal to the elastic stiffness. Due to the gap between the supporting medium and the fastener, the slope of #4 tends to be vertical and is conventionally set to 10 times K_h in the analyses. The separation points between #4 and #6, and between #6 and #40, depend upon the force on the backbone curve and are updated at every hysteresis cycle. Further information on the hysteresis model employed in the analyses can be found in [16].

2.3 WITHDRAWAL STRENGTH

The withdrawal strength of the fastener is modelled with a third set of non-linear springs (green springs in Figure 1), uniformly distributed along the shank. Each spring is restrained to a master node, located in the centre of the beam where it is attached and to a fixed point of the surrounding space.
These springs have a non-symmetric force-displacement relationship (Figure 4). If loaded in tension, an elasto-plastic behaviour is adopted with elastic stiffness K_{ax} and withdrawal load F_{ax}. The inelastic branch has a softening behaviour, determined by assuming that the strength at the ultimate displacement $V_{u,ax}$ (with $V_{u,ax}$ equal to 10 times the yield displacement) is 80% of F_{ax}.

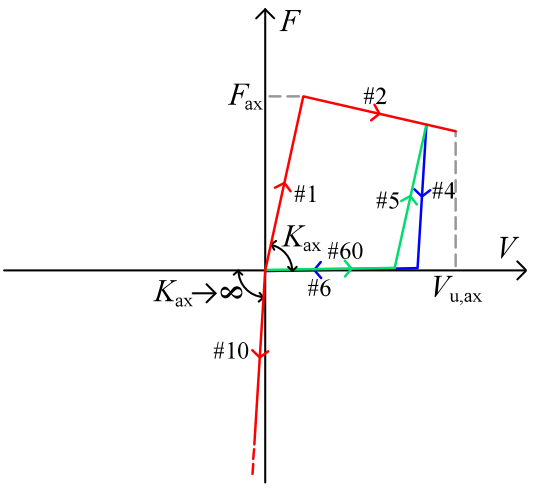

Figure 4: *Withdrawal behaviour of the fastener: piecewise-linear law of the non-linear springs (backbone curve in red, unloading path in blue and reloading path in green).*

The hysteretic behaviour of these spring is similar to the one described in Section 2.2. The slope of branch #4 should tend to infinite as, once extracted, the steel plate cannot push the fastener back inside the timber element. Therefore, branch #4 simulates the sudden reduction of load-carrying capacity due to the gap between the metal plate and the fastener cap.
It should be also noticed that, using the schematization presented in Figure 1, the fastener cannot penetrate the timber medium; for this reason, if the spring is loaded in compression, a very stiff elastic behaviour is adopted.

3 M1-MODEL CALIBRATION

The design rules presented below are used to calibrate a M1-model simulating a steel-to-timber joint with an annular-ringed shank nail manufactured by Simpson Strong-Tie (Figure 5). These rules are taken partly from Eurocode 5 [4] and from the European Technical Approval (ETA) of the fastener [5].

Figure 5: *Annular-ringed shank nails (reproduced from [11]).*

It should be noticed that those rules lead to a prediction of the characteristic strength capacities of the joint and were derived under the assumption of an ideal-plastic behaviour. However, an elasto-plastic behaviour based on the average strength capacities is used when investigating the actual behaviour of the joint. Therefore, average values of the strength capacities are obtained in accordance with Equation 1, assuming a standard normal distribution.

$$f_m = \frac{f_k}{\left(1 - 1.645 \cdot COV\left[f_k\right]\right)} \tag{1}$$

In the equation above, f_m is the average value of the strength while f_k and $COV\left[f_k\right]$ denote its characteristic value and the coefficient of variation of such quantity.

3.1 YIELD MOMENT

The characteristic yield moment of the fastener ($M_{y,Rk}$) was defined in agreement with the design model given in Eurocode 5 [4]:

$$M_{y,Rk} = 0.30 f_{u,k} d^{2.6} \tag{2}$$

In the previous equations, d denotes the diameter of the fastener while $f_{u,k}$ signifies its ultimate tensile strength, set to $f_{u,k}$ = 600 N/mm^2 in the calculation. It should be noticed that specific calculation models for fasteners with profiled shank have not been derived yet. Therefore, for realistic joint design, the yield moment of those fasteners should be assessed as prescribed in [3].

3.2 EMBEDDING LOAD OF TIMBER

The embedding load was determined by multiplying the tributary area of each beam element (i.e. $d \times l$) by the characteristic embedding strength of timber $f_{h,k}$:

$$F_{h,Rk} = f_{h,k} dl = 0.082 \rho_k d^{0.7} l \quad (3)$$

The characteristic embedding strength $f_{h,k}$ was defined according to the Eurocode 5 [4] model.

3.3 WITHDRAWAL LOAD

The withdrawal load was determined in a similar way to what presented in Section 3.2, i.e. by multiplying the tributary area of each beam element by the withdrawal parameter of the fastener $f_{ax,k}$. Here, the tributary area of each beam is determined on the basis of the threaded length of the shank and the discretization of the model, by multiplying the l_{thr} over n_{el} ratio by the diameter of the fastener d:

$$F_{ax,Rk} = f_{ax,k} d \frac{l_{thr}}{n_{el}} \quad (4)$$

where the symbol n_{el} denotes the number of beam elements used to simulate the fastener shank.
The withdrawal parameter depends upon the geometry of the fastener (i.e. threaded length and diameter) and the density of timber. The current version of Eurocode 5 [4] does not include any design provision for the prediction of this parameter and the use of harmonized technical specifications is required; therefore, the withdrawal parameter $f_{ax,k}$ used in the analyses was determined according to the rules included in [6].

3.4 STIFFNESS PROPERTIES

Calculation models for the prediction of the embedment stiffness of timber and of the withdrawal stiffness of the nail have not been derived to date. These properties depend upon the fastener geometry (diameter, profiled surface, etc.) and the density of the timber element in which it is embedded. However, detailed information on those stiffness properties have not been published yet.
In the following, values of K_h and K_{ax} were estimated from test results: K_h was determined multiplying the tributary area of each beam (i.e. $d \times l$) by a foundation value estimated from the results published in [12, 13] and set to 25 N/mm^3. Similarly, the withdrawal stiffness K_{ax} was assessed from the results published in [11] multiplying the tributary area by a foundation value equal to 7 N/mm^3. The influence of those properties on the global response of the joint is discussed in Section 6.

4 M2-MODEL DESCRIPTION

As highlighted in Section 2, results obtained on single fastener joints could be employed to analyse systems where many of them are present (e.g. a metal connector). Due to the simultaneous presence of several springs and components, it is suggested that the analyses are carried out by means of a simplified schematization of the steel-to-timber joint less computationally demanding. Here, a second hysteresis model is proposed (in the following referred to as M2-model) in which the non-linear response of the joint is lumped into a unique spring element.
The M2-model (Figure 6) represents the steel-to-timber joint as a two-node spring element with three degrees of freedom. Two degrees of freedom (blue and red spring) simulate the mechanical behaviour in parallel and perpendicular to the grain direction; the third degree of freedom (green spring) simulates the withdrawal strength under tensile loads.

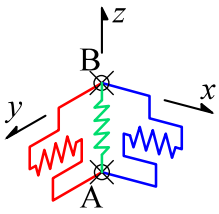

Figure 6: *Schematics of a steel-to-timber joint simulated with the M2-model.*

This model is restrained on one end (point A) to the 3D element that simulates the timber part where the fastener is embedded and on the other end (point B) on the connector at the fastener cap location.
The M2-model can be calibrated either on the numerical results obtained with other hysteresis model (for instance using the M1-model discussed above) or on calculated strength and stiffness values determined either from analytical formulas or from experimental tests.

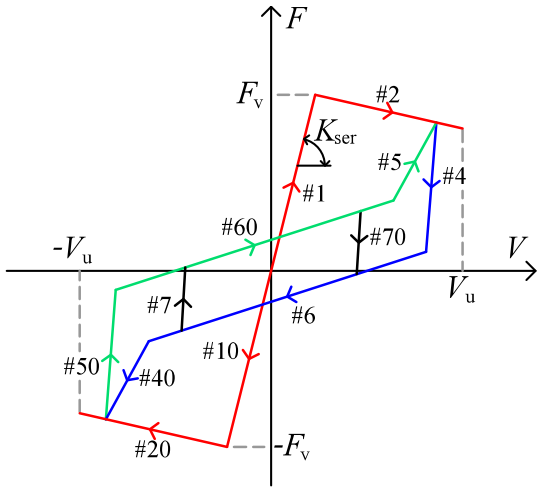

Figure 7: *Shear behaviour of the joint: piecewise-linear law of the non-linear springs (backbone curve in red, unloading path in blue and reloading path in green).*

The piecewise-linear law used to characterize the shear behaviour of the M2-model is given in Figure 7; a bilinear backbone curve is adopted, with elastic stiffness K_{ser} and load-carrying capacity F_v. The inelastic branch is characterized by a softening behaviour and is determined by assuming that the strength at the ultimate displacement V_u is 20% lower than F_v (with V_u set 10 times the yield displacement). The piecewise-linear branches presented in Figure 7 follow the same rules described in the previous sub-sections.

Stiffness degradation and hysteretic pinching in joints with dowel-type fasteners are due to slackness or loosening caused by cyclic loadings; in fact, the pinching effect is caused by a reduction of stiffness at small joint displacement, where a cavity is formed around the fastener by timber crushing [9]. Without the support of the timber, the fastener shank provides the resistance to the applied load. Stiffness increases as the fastener gets in contact again with the surrounding timber at increased deformation levels.

The withdrawal resistance of the joint under tensile loads is simulated with a hysteresis model similar to the one presented in Figure 4. It should be noticed that the metal connector is not allowed to penetrate the timber member where the fastener is embedded (and to which is in contact). Therefore, branch #10 is not activated.

5 M2-MODEL CALIBRATION

The design rules presented below are used to calibrate a M2-model simulating a nailed steel-to-timber joint with an annular-ringed shank nail (Figure 5) manufactured by Rothoblaas. Similarly with what was done in Section 3, the model is calibrated on the design rules given in Eurocode 5 [4] and in the European Technical Approval of the fastener used in the analyses [8]. Average values of the characteristic strength capacities were determined according to Equation 1.

5.1 SHEAR BEHAVIOUR

The instantaneous slip modulus (K_{ser}) of the M2-model was determined according to the design rules prescribed in Eurocode 5 [4]:

$$K_{ser} = 2\rho_m^{1.5} d^{0.8} / 30 \tag{5}$$

where ρ_m is the average density of the timber panel and d is the diameter of the fastener. The factor 2 adopted in Equation 5 is derived basing on mechanical relationships and considers the clamping of the nail cap to the metal plate.

The load-carrying capacity ($F_{v,Rk}$) of the M2-model was determined according to the design rules included in [8]:

$$F_{v,Rk} = F_{lat,Rk} + 0.50 F_{ax,Rk} \tag{6}$$

where $F_{lat,Rk}$ is the characteristic lateral dowel-capacity of the nailed steel-to-timber joint while $F_{ax,Rk}$ represents the characteristic withdrawal strength of the nailed joint. The characteristic lateral dowel-capacity for a steel-to-timber joint with thick plate is given by the lowest value among those obtained with Equation 7.

$$F_{lat,Rk} = \min \begin{cases} f_{h,k} t_1 d & \text{(a)} \\ f_{h,k} t_1 d \left[\sqrt{2 + \dfrac{4 M_{y,Rk}}{f_{h,k} t_1^2 d}} - 1 \right] & \text{(b)} \\ 2.3 \sqrt{M_{y,Rk} f_{h,k} d} & \text{(c)} \end{cases} \tag{7}$$

where $f_{h,k}$ is the embedding strength of timber given in Eurocode 5 [4], t_1 is the penetration depth while d and $M_{y,Rk}$ represent the diameter and the yield moment of the fastener, respectively.

The second term in Equation 6 is the contribution due to the rope effect. It should be noted that Equation 6 takes into account a rope effect equal to 50% of the characteristic withdrawal strength of the nailed joint. On the contrary, the design model included in Eurocode 5 [4] was derived for fasteners with smooth shank and limits such effect to 25% the characteristic withdrawal capacity $F_{ax,Rk}$. The characterization of the withdrawal capacity of the nailed joint is discussed in the following sub-section.

5.2 WITHDRAWAL BEHAVIOUR

The withdrawal stiffness depends upon the grip between the profiled shank and the surrounding timber. Specific model for the prediction of such stiffness values have not been derived yet. Similarly with what presented in Section 3.4, the stiffness properties used in the analyses were derived based on the results published in [11]. In particular, the authors found that the loading curves have a linear trend until the yield load, a peak at around 2 mm of displacement, and a distinct load decrease after the displacement corresponding to the peak load.

The characteristic withdrawal strength of the nailed joint was defined as:

$$F_{ax,Rk} = f_{ax,k} l_{thr} d \tag{8}$$

where $f_{ax,k}$ is the withdrawal parameter, d the diameter of the fastener and l_{thr} the threaded length of the shank.

Characteristic values of the withdrawal parameter were determined according to the design rules included in [8].

6 RESULTS AND DISCUSSIONS

Numerical simulations were carried out using the finite elements software package *ABAQUS* [17]. Analyses highlighted the potentials of the proposed models and pointed out issues and current challenges on numerical modelling of steel-to-timber joints with dowel-type fasteners. As mentioned in the introduction, the springs used in the M1- and M2-model were simulated using a user element subroutine (UEL) [16].

6.1 SIMULATIONS ON THE M1-MODEL

Monotonic and cyclic simulations were performed on a steel-to-timber joint with an annular ringed shank nail

manufactured by Simpson Strong-Tie. Analyses were carried out in displacement control with a 4 mm thick metal plate and a nail with d = 4.0 mm, l_{thr} = 44 mm and t_1 = 54 mm [5].

At first the characteristic lateral dowel capacity ($F_{lat,Rk}$) was investigated. Numerical analyses were performed by varying the characteristic density of timber (between 300 kg/m^3 and 500 kg/m^3) and were repeated for two more joints, assembled using similar fasteners but with larger diameters (the first with d = 6.0 mm and the latter with d = 8.0 mm). The lateral dowel capacity was assessed as the maximum load achieved by the joint before the activation of the rope effect.

Results of this study are summarized in Figure 8, where the numerical prediction of the lateral dowel capacities are compared to the calculated values determined with Equation 7, showing an excellent correspondence.

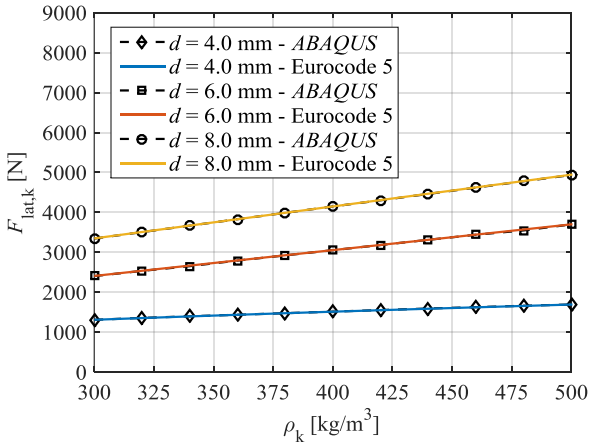

Figure 8: *Characteristic lateral dowel capacity of a steel-to-timber joint with an annular-ringed shank nail: comparison between numerical results and analytical predictions.*

Simulations carried out with d = 4.0 mm led to a plastic deformed configuration where the bending capacity was attained with two plastic hinges together with embedding of timber (mode *c* according to Equation 7). It should be noticed that the calculated values of $F_{lat,Rk}$ were assessed with a factor 2.0 instead of the 2.3 given in Equation 7, as the enhancing contribution due to the rope effect is neglected. Simulations performed with d = 6.0 mm and d = 8.0 mm led to higher lateral dowel capacities and to a plastic deformed configuration where the bending capacity was attained with a plastic hinge together with embedding of timber (mode *b* according to Equation 7).

The mechanical behaviour of the joint under monotonic loads was investigated afterwards. Average values of the strength capacities were assessed according to Equation 1, assuming a coefficient of variation equal to 10% for all the strength capacities. Simulations were performed with the d = 4.0 mm nail, considering a characteristic density ρ_k = 350 kg/m^3 (ρ_m = 420 kg/m^3, as prescribed in [2] for softwood species with strength class C24). At first the withdrawal stiffness was kept constant (with a foundation modulus k_{ax} = 7 N/mm^3) and the embedding stiffness of timber was varied with values between 25 N/mm^3 and 75 N/mm^3.

The embedding stiffness was kept constant afterwards (with modulus k_h = 25 N/mm^3) while the withdrawal stiffness was varied with values between 7 N/mm^3 and 70 N/mm^3.

Results of this study are summarized in Figure 9 and 10.

Simulations where the embedment stiffness of timber was varied (Figure 9) showed a little increase of the elastic stiffness which led also to a slightly higher load-carrying capacity. On the contrary, simulations where the withdrawal stiffness was varied led to small variations of the loading curve between 3 mm and 8 mm of displacement; the initial stiffness, as well as the load-carrying capacity, did not show significant dependency upon this parameter.

Compared to similar results published by [11], the yield point is achieved at a much lower load than what was observed in the tests and the peak strength is both lower and achieved at a much higher displacement (at around 21 mm instead of the 13 mm observed in the tests [11]).

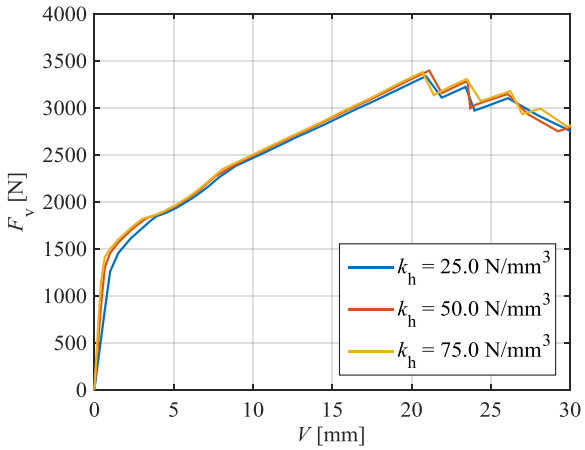

Figure 9: *Load-carrying capacity of a steel-to-timber joint with an annular-ringed shank nail when the embedment stiffness is varied and the withdrawal stiffness is kept constant.*

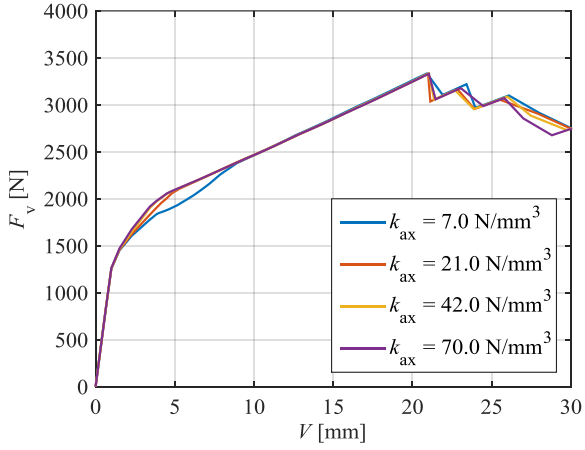

Figure 10: *Load-carrying capacity of a steel-to-timber joint with an annular-ringed shank nail when the withdrawal stiffness is varied and the embedment stiffness is kept constant.*

Further studies suggested that those differences might be minimized by introducing an additional spring element, applied in the direction of the nail shank and used to simulate the friction between fastener and timber.

Finally, the steel-to-timber joint was simulated in cyclic conditions. The analysis was carried out by considering the fastener with d = 4.0 mm, ρ_k = 350 kg/m^3 (corresponding to a ρ_m = 420 kg/m^3), k_{ax} = 7 N/mm^3 and k_h = 25 N/mm^3. The displacement schedule used in the simulation was determined in agreement with [10], assuming an ultimate displacement of 30.0 mm.

Results of this simulation are presented in Figure 11. The pinching effect was developed as the gaps between supporting medium and fastener are formed. It should be noticed that typical features of joints in timber structures like the strength and stiffness degradation were not considered in the simulation but might be included in future developments of this study and implemented in the model by means of specific input parameters in the UEL used in the analysis [16].

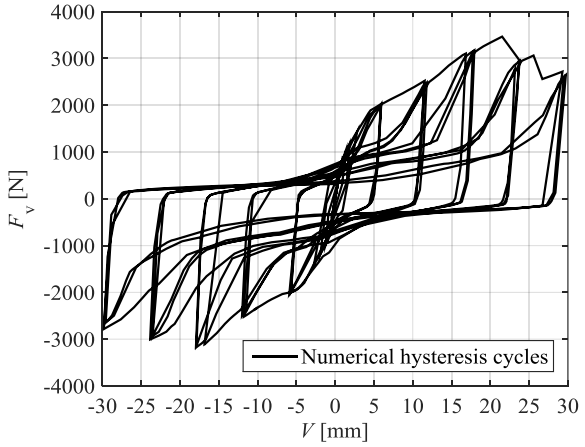

Figure 11: *Hysteretic behaviour of a steel-to-timber joint with an annular-ringed shank nail.*

6.2 SIMULATIONS ON THE M2-MODEL

Monotonic simulations were carried out on a wall-to-floor connection assembled with a Rothoblaas TTF200 angle-bracket [7] (Figure 12) and tested at the University of Trento [1, 14, 18]. The TTF200 connector was anchored to the CLT panels using 60 Rothoblaas annular-ringed shank nails (30 in each panel) [8].

The nails were simulated using the M2-model presented before and calibrated on the rules given in Section 5. A characteristic density ρ_k = 385 kg/m^3 was used in the calculations (with ρ_m = 460 kg/m^3). Average values of the strength capacities were determined according to Equation 1, with a coefficient of variation of 10%.

The metal connector and the first board layer of the CLT panels were accounted in the model and meshed using 8-node brick elements with reduced integration (C3D8R elements). It should be noted that the timber panels were introduced in the simulations to account for the surface-to-surface contact interaction and do not affect the behaviour of the system.

Timber was modelled as an equivalent-elastic isotropic material with E = 0.6 GPa and ν = -0.57. Steel was modelled as an elasto-plastic material with E = 210 GPa, ν = 0.3 and f_y = 230 MPa.

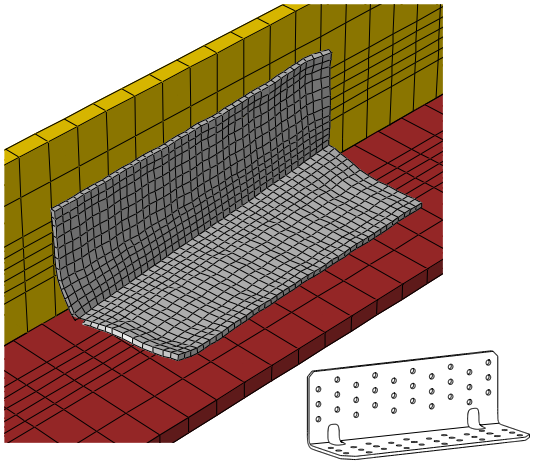

Figure 12: *Deformed view of the connection considered in the simulations (bottom: schematics of the TTF200 angle bracket, reproduced from [7]).*

Monotonic shear tests were carried out considering two different spring calibrations: (*a*) a unique calibration for each group of springs, defined on the average strength capacities (identical values for all the spring that simulate the mechanical behaviour in parallel to grain direction of a board layer); (*b*) by calibrating each spring with predefined values of K_{ser} and F_{max}, determined from the average quantities by considering a scatter of mechanical properties.

Analyses were repeated afterwards by modifying the calculation model used to predict the instantaneous slip modulus K_{ser} of the joint, i.e. by substituting the factor 2 considered in the Eurocode 5 [4] model with a factor 1. This modification was motivated by the results presented in [11].

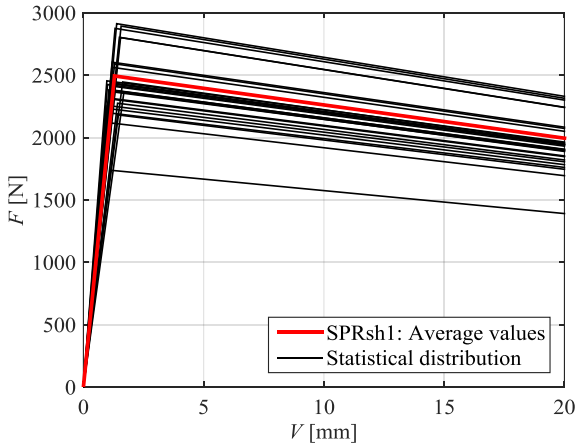

Figure 13: *Backbone curve determined on the average values of the strength (red line) and backbone curves generated by considering a predefined coefficient of variation (black lines).*

Figure 13 compares the backbone curve determined on the average values of the strength capacities (red line)

and 30 backbone curves (black lines) generated from the previous one, assuming a coefficient of variation equal to 10%. As visible from the same figure, the same scatter of properties was also considered when defining the elastic stiffness of the backbone curves; however, its influence was not investigated in detail in this study.
Figure 14 compares experimental (black and grey lines) and numerical results (dashed and dash-dot lines with various colours). It is clearly visible that analyses carried out with the Eurocode 5 [4] model for the prediction of K_{ser} (blue dashed line and purple dash-dot line) lead to a much stiffer systems compared to those experimentally tested. A more reliable prediction was obtained with the modified model (magenta dashed line and orange dash-dot line), where the factor 2 was reduced to 1. The maximum bearing capacity measured in the tests showed little differences compared to those obtained in the numerical simulations. In particular, the value obtained assuming a statistical distribution of properties and the modified model for the prediction of K_{ser} are very close to the values found with experimental tests.

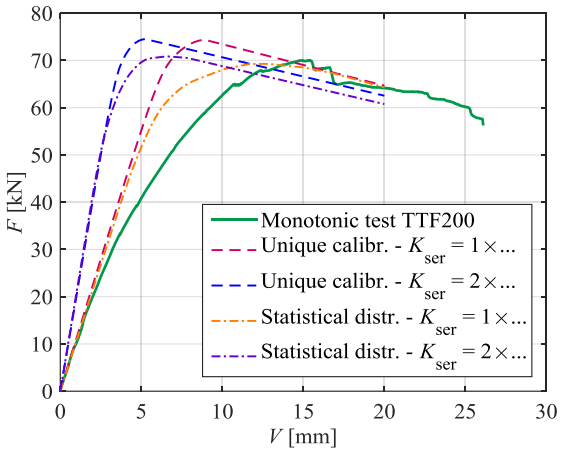

Figure 14: *Monotonic shear tests on a wall-to-floor connection with a Rothoblaas TTF200 angle bracket and 60 threaded nails: comparison between experimental and numerical results.*

Finally, it should be noticed that the backbone curve used to calibrate the mechanical behaviour of the nails has a bilinear representation and might have a significant influence on the shape of the loading curve determined in the simulations. Therefore, with the aim to obtain more reliable results, future developments of this study should consider a trilinear backbone curve instead of the bilinear adopted here, and should investigate the mechanical behaviour under cyclic loads.

7 CONCLUSIONS

The mechanical behaviour of steel-to-timber joints with annular-ringed shank nails was investigated.
At first a general hysteresis model (labelled M1-model) for the prediction of the mechanical behaviour of single steel-to-timber fastener joints with dowel-type fasteners was presented and calibrated in the case of an annular-ringed shank nail. The joint is schematized as an elasto-plastic beam in a non-linear medium characterized by a compression-only behaviour and simulates the non-linear response by means of a component approach.
A second hysteresis model is presented afterwards (labelled M2-model), in which the joint is schematized by a two-node spring element with three degrees of freedom. Two degrees of freedom simulate the shear behaviour in parallel and perpendicular to the grain direction; the third one simulates its behaviour under tensile loads.
It should be noticed that results obtained on single joints (by means of the M1-model) could be employed to analyse systems where many fasteners are present (with the M2-model). For instance, results obtained on nailed steel-to-timber joints could be implemented in a more general model to predict the behaviour of a metal connector like a hold-down or an angle bracket.
Numerical analyses were subsequently carried out on two reference systems: a single steel-to-timber joint and a wall-to-floor connection with an angle bracket and 60 nails. Those analyses aimed at highlighting the potentials of the proposed models and to set future challenges that need to be addressed to improve the results obtained with numerical modelling. The scatter of mechanical properties was also taken into account in the simulations and a stochastic approach was proposed.

ACKNOWLEDGEMENTS

The models presented in the paper were developed while Matteo Izzi was collaborating as research assistant at the CNR IVALSA *Trees and Timber Institute* of S. Michele all'Adige, Italy. The financial support of the *Trees and Timber Institute* is gratefully acknowledged.

REFERENCES

1. Casagrande D, Polastri A, Sartori T, Loss C (2016) Experimental campaign for the mechanical characterization of connection systems in the seismic design of timber buildings. *World Conference on Timber Engineering (WCTE)*, Vienna, Austria.
2. EN 338 (2009) Structural timber - Strength classes. CEN, Brussels, Belgium.
3. EN 409 (2009) Timber structures. Test methods. Determination of the yield moment of dowel type fasteners. CEN, Brussels, Belgium.
4. EN 1995-1-1:2004/A2 (2014) Eurocode 5: Design of timber structures. Part 1-1: General. Common rules and rules for buildings. CEN, Brussels, Belgium.
5. ETA-04/0013 (2013) European Technical Approval. CNA Connector nails, PCR Connector nails and CSA Connector screws. ETA, Brussels, Belgium.
6. ETA-06/0106 (2013) European Technical Approval. Three-dimensional nailing plate (timber-to-timber/timber-to-concrete angle bracket). ETA, Brussels, Belgium.

7. ETA-11/0496 (2013) European Technical Approval. Three-dimensional nailing plate (Angle Bracket for timber-to-timber or timber-to-concrete or steel connections). ETA, Brussels, Belgium.
8. ETA-13/0523 (2013) European Technical Approval. GH screws and GH ring shanked nails. ETA, Brussels, Belgium.
9. Foliente GC (1995) Hysteresis Modeling of Wood Joints and Structural Systems. *Journal of Structural Engineering*, **121**(6): 1013-1022, doi: 10.1061/(ASCE)0733-9445(1995)121:6(1013).
10. ISO 16670 (2003) Timber Structures. Joints made with mechanical fasteners. Quasi-static reversed-cyclic test method. ISO, Geneva, Switzerland.
11. Izzi M, Flatscher G, Fragiacomo M, Schickhofer G (2016) Experimental investigations and design provisions of steel-to-timber joints with annular-ringed shank nails for Cross-Laminated Timber structures. *Construction and Building Materials (under review)*.
12. Karagiannis V, Málaga-Chuquitaype C, Elghazouli AY (2016) Proposal of an analytical procedure and a simplified numerical model for elastic response of single-storey timber shear-walls. *Construction and Building Materials*, **102**: 1168-1179, doi: doi:10.1016/j.conbuildmat.2015.09.021.
13. Pedersen MU (2002) Dowel Type Timber Connections - Strength modelling. *Ph.D. Thesis*. Technical University of Denmark, Copenhagen, Denmark.
14. Polastri A, Pozza L, Loss C, Smith I (2015) Structural characterization of multi-storey CLT buildings braced with cores and additional shear walls. *INTER 2015 Meeting*, Šibenik, Croatia, Paper 48-15-5.
15. Rinaldin G (2012) Non-linear analysis and modelling of masonry and timber (in Italian). *Ph.D. Thesis*. University of Trieste, Trieste, Italy, http://www.openstarts.units.it/dspace/handle/10077/8643.
16. Rinaldin G, Amadio C, Fragiacomo M (2013) A component approach for the hysteretic behaviour of connections in cross-laminated wooden structures. *Earthquake Engineering & Structural Dynamics*, **42**(13): 2023-2042, doi: 10.1002/eqe.2310.
17. Simulia DS (2012) *ABAQUS 6.12 Documentation*. Providence, Rhode Island, USA.
18. Tomasi R, Smith I (2015) Experimental Characterization of Monotonic and Cyclic Loading Responses of CLT Panel-To-Foundation Angle Bracket Connections. *Journal of Materials in Civil Engineering*, **27**(6): 04014189(1-10), doi: 10.1061/(ASCE)MT.1943-5533.0001144.